

Biocomputing: numerical simulation of glioblastoma growth using diffusion tensor imaging

Pierre-Yves Bondiau^{1,2}, Olivier Clatz^{1,3}, Maxime Sermesant¹,
Pierre-Yves Marcy², Herve Delingette¹, Marc Frenay⁴
and Nicholas Ayache¹

¹ Institut National de Recherche en Informatique et Automatique, 2004 Route des Lucioles, 06 902 Sophia Antipolis, France

² Département de Radiothérapie, Centre Antoine Lacassagne, 33 av de Valombrose, 06189 Nice, France

³ Surgical Planning Laboratory, Brigham and Women's Hospital, 75 Francis Street Boston, MA 02115, USA

⁴ Département d'Oncologie Médicale, Centre Antoine Lacassagne, 33 av de Valombrose, 06189 Nice, France

E-mail: pierre-yves.bondiau@cal.nice.fnclcc.fr

Received 20 July 2007, in final form 20 December 2007

Published 15 January 2008

Online at stacks.iop.org/PMB/53/879

Abstract

Glioblastoma multiforma (GBM) is one of the most aggressive tumors of the central nervous system. It can be represented by two components: a proliferative component with a mass effect on brain structures and an invasive component. GBM has a distinct pattern of spread showing a preferential growth in the white fiber direction for the invasive component. By using the architecture of white matter fibers, we propose a new model to simulate the growth of GBM. This architecture is estimated by diffusion tensor imaging in order to determine the preferred direction for the diffusion component. It is then coupled with a mechanical component. To set up our growth model, we make a brain atlas including brain structures with a distinct response to tumor aggressiveness, white fiber diffusion tensor information and elasticity. In this atlas, we introduce a virtual GBM with a mechanical component coupled with a diffusion component. These two components are complementary, and can be tuned independently. Then, we tune the parameter set of our model with an MRI patient. We have compared simulated growth (initialized with the MRI patient) with observed growth six months later. The average and the odd ratio of image difference between observed and simulated images are computed. Displacements of reference points are compared to those simulated by the model. The results of our simulation have shown a good correlation with tumor growth, as observed on an MRI patient. Different tumor aggressiveness can also be simulated by tuning additional parameters. This work has demonstrated

that modeling the complex behavior of brain tumors is feasible and will account for further validation of this new conceptual approach.

(Some figures in this article are in colour only in the electronic version)

Introduction

The incidence of central nervous system (CNS) primary malignant and secondary tumors has been increasing over the last 25 years for all age categories, whereas mortality rate has decreased for people younger than 65 years old (Legler *et al* 1999).

The majority of CNS primary tumors is of glial, astrocytic or oligodendroglial origin. The treatment of these tumors is based on surgery, radiotherapy and/or chemotherapy. However, the current treatment of high grade cerebral tumors is disappointing (Mineo *et al* 2007, Fazy-Dorner *et al* 2003, Jeremic *et al* 2003). Anaplastic astrocytoma and glioblastoma multiforma (GBM) are among the most aggressive tumors. In spite of ongoing research and various treatment protocols, overall survival is about a year. Overall survival is similar regardless of the treatment. Radiotherapy alone is a reasonable option (Miralbell 1999). The role of chemotherapy in adjuvant treatment and in the treatment of tumor recurrence is currently questionable: the additional benefit varies among the published series in the literature and seems to be low (Wolff *et al* 1999, Frenay *et al* 2000). Patients with high-grade astrocytomas have also been treated with 3D treatment planning and high-dose conformal radiotherapy (Lee *et al* 1999a). These high-dose conformal radiotherapy protocols did not improve survival, but altered the pattern of relapse (Nakagawa 1998) since fewer local failures were observed.

A better understanding of tumor cell diffusion in the brain may help to interpret these results. This can be achieved by numerical simulation of both tumor growth and tumor cell diffusion. Moreover, feeding that simulation to individual data (i.e. patient data) may allow the generation of personalized simulations.

Previous models of GBM growth pattern have been described in the literature and were based either on Gompertz's theory (Swanson *et al* 2002a, Tracqui *et al* 1995, Deisboeck *et al* 2001) or biomechanical models (Kyriacou *et al* 1999). A more complicated model simulates both tumoral growth and diffusion (Woodward *et al* 1996). Computer simulation of tumor growth will allow quantitative and qualitative comparison with histological reality, and provide additional information concerning tumoral spread (i.e. microscopic invasion).

The aim of this work was to develop a model of GBM growth for better understanding. GBM growth can be represented by two components—a mechanical component with a mass effect on surrounding brain structures and an invasive component that infiltrates brain structures.

The first component is incorporated to the model by using different biomechanical parameters for different cerebral structures (skull, falx, ventricles, gray and white matter), while the second one uses the architecture of white matter fibers estimated by diffusion tensor imaging (Ruiz-Alzola *et al* 2002).

The main improvement of our model is the use of diffusion tensor imaging to determine the preferred direction of diffusional tumor extension. A relation between mechanical and diffusion components is described. We tuned the parameter set of the method to calibrate the model on patient images with patients' MRI.

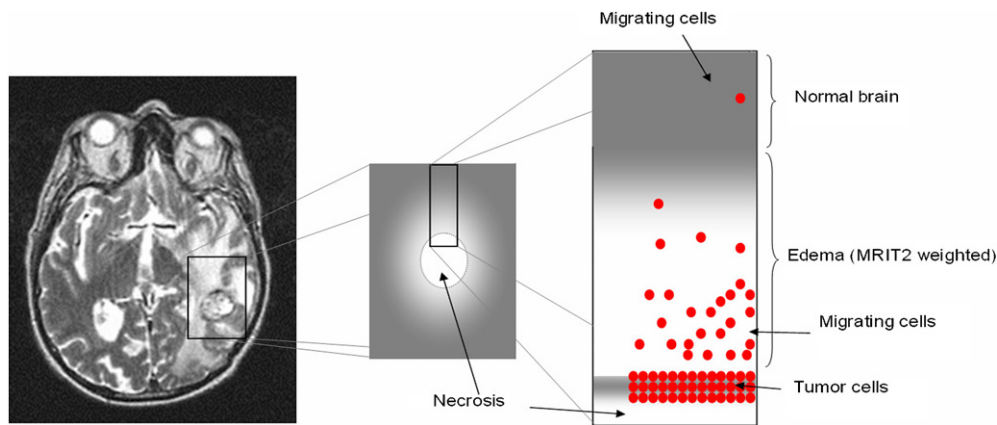


Figure 1. Theoretical relation between T2 weighted MRI and tumor infiltration. Left: tumor image on T2 MRI. Center: theoretical T2 weighted MRI centered on the tumor. Right: zoom on tumor section (from bottom to top: necrosis, wall of active cells, migrating cell responsible for edema and isolated migrating cells in the normal brain).

Previous work on tumor growth

Tumor growth results from tumor cell division. After each cell cycle, the cell population doubles. After C cycles, the number of cells will be multiplied by 2^C . Exponential growth describes the population density $N(t)$ at any time in terms of the initial population density (0) at time $t = 0$ and at the growth rate constant k . The experimental growth is later limited to an asymptotic rate:

$$P(t) = M \exp(-\alpha \exp(-Mkt)) \quad (1)$$

where

- $\alpha = \ln(M/P_0) \exp(Mkt)$ with P_0 the initial population,
- P is the population density,
- t is the time,
- k is the cell growth rate and
- M is the maximum sustainable population.

Tumor growth results from an imbalance between cell proliferation and cell death. Moreover, malignant tumors consist of different cellular clones with different growth properties and behaviors (Kansal *et al* 2000a). Therefore, tumor growth is more often unforeseeable or anarchistic and it is difficult to imagine that all tumors conform to simple rules (Retsky *et al* 1990, Patel *et al* 2001, Bussemaker *et al* 1997, Kansal *et al* 2000b, 2000c, 2000d).

Case of GBM

GBM are brain tumors with a central necrosis, peripheral tumor cells and migrating cells responsible for edema (MRI T2 weighted). Further, in the brain periphery there are not enough migrating cells to trigger the edema reaction (Kantor *et al* 2001) (see figure 1). Since GBM can exhibit different growth rates, it is challenging to find the best model parameters to characterize the local or global tumor aggressiveness.

Previous publications on glioma modeling isolate two key features: a proliferation component and a diffusion component (Tracqui 1995, Swanson *et al* 2002b). The diffusive

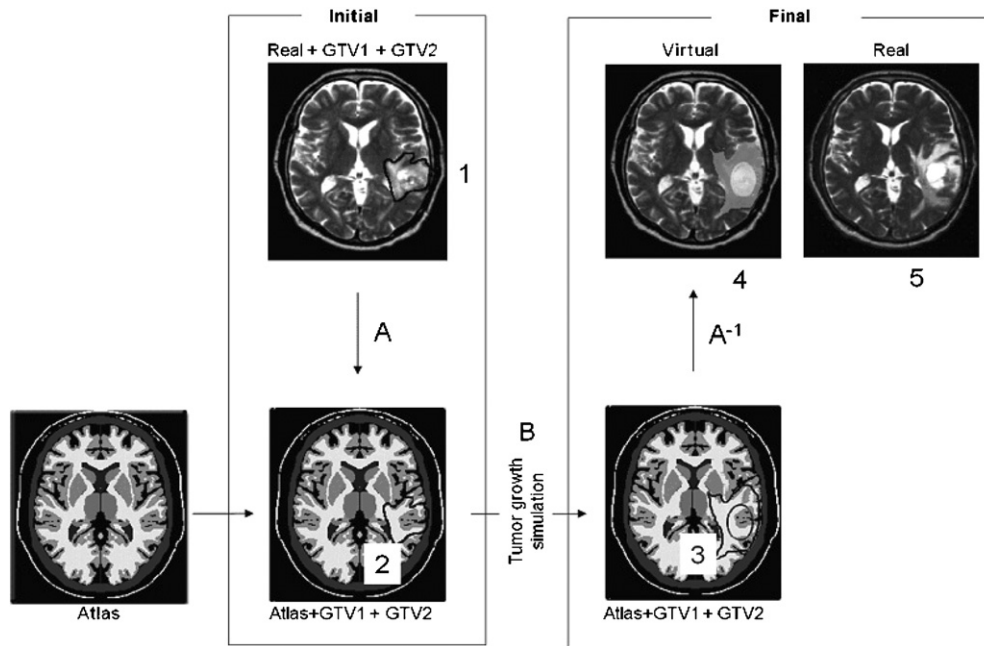


Figure 2. Flowchart of the method. All patients' MRIs were previously transformed using an automatic rigid matching method with the atlas to fit patients' MRI with atlas geometry. Segmentation (GTV1+GTV2) of the tumor was made on initial MRI (1) and was match (A) onto the atlas (2). Then the tumor grew (B) until six months later on the atlas and created local deformations (3) and invasion. Finally, we reported deformations and new tumor volume on the patients' initial MRI. Comparisons were made between this MRI and the real patient MRI (5).

model proposes a macroscopic way to describe tumor growth. Conservation equations were formulated by Murray (Swanson *et al* 2002c, Murray 2002):

$$\partial c \frac{\partial c}{\partial t} = -\text{div}(J) + S(c, t) - T(c, t) \quad (2)$$

where

- c represents the tumor cell density,
- J represents the diffusion pattern of tumor cells,
- $S(c, t)$ represents the source factor tumor cells function and
- $T(c, t)$ models the efficacy of anti-tumor treatment.

The proliferation component generates new matter which has a mechanical volume effect on the brain and pushes back brain structures according to their elasticity. The diffusion component invades adjacent structures and is responsible for infiltration of white and gray matter. The interaction between these two components defines the virtual glioma (VG) growth.

Material and methods

To set our model, we have compared simulated VG growth (initialized with patients' data) with observed growth in MRI patients. To tune the parameter set of the method, we use the steps presented in the flowchart (see figure 2).

Table 1. Image sequences of T1 weighted MRI and T2 weighted MRI.

MRI	T1W, T1W with contrast	T2W
TE (ms)	1.7	102
TR (ms)	7.9	5000
Band width 5 (kHz)	15.153	31.25
FOV (cm)	26	26
Excitation	2	2

Table 2. Image characteristics of atlas MRI, T1 weighted MRI, T2 weighted MRI and diffusion tensor imaging (DTI).

MRI	Atlas MRI	T1W, T1W with contrast	MR1 T2W	DTI
XDIM	181	256	256	256
YDIM	217	256	256	256
ZDIM	181	60	64	36
TYPE	Signed fixed	Unsigned fixed	Unsigned fixed	Signed fixed
PIXSIZE	16 bits	16 bits	16 bits	
VX (mm)	0.6	1.015 623	1.015 641	1.0
VY (mm)	0.6	1.015 625	1.015 625	1.0
VZ (mm)	0.6	2.000 000	1.900 000	4.0
Field (mm)		173 × 230	173 × 230	

Pre-processing. All MRIs from our patients are matched with the atlas using an automatic (mutual information) rigid matching so that MRI patients can be resampled in the atlas geometry.

Patients

Standard imaging protocols for brain tumor radiotherapy were used for this study. MRI acquisitions used a head coil, and three sequences (T1, T2 and T1 with gadolinium injection) were performed. For this work, we used a typical case of localized glioma. Images were exported in a Dicom-3 format. Image characteristics are shown in tables 1 and 2. These MRIs were performed during standard follow-up analyses following treatment. At the time of the initial set of image, a patient was asymptomatic and refused any specific treatment. Yet, he accepted to have an MRI six months later. At that time, the second MRI showed a tumor progression (figure 2) and the patient was symptomatic. Then, the patient accepted a multimodality treatment including surgery, chemotherapy and radiotherapy.

Tumor segmentation

To develop a customized model of tumor growth, the delineation of the tumor in a patient's image is mandatory. This step was conducted manually by a medical expert on the patient's initial MRI. We assumed that tumor segmentation error was minimal as compared to the size of the tumor. The tumor volume was defined as the area of the hypersignal observed into MRI. It was split into two parts as recommended in some protocols for radiotherapy treatment. Gross tumor volume 1 (GTV1) was delineated in T1-weighted MRI after gadolinium injection (MRI-T1i). The hypersignal in the MRI-T1i sequence shows the proliferate volume of the tumor. Tumor cell (alive or dead by necrosis or apoptosis) density in GTV1 represents 100%. Gross

tumor volume 2 (GTV2) was delineated on T2-weighted MRI (MRI-T2). The hypersignal in MRI-T2 shows edema volume. GTV2 took not only the GTV volume, but also the volume of edema where the migrating tumor cells are very likely to be present. This edema is usually surrounding the tumor, and is visualized as a hypersignal on T2-weighted MRI. We assume that less than 5% of tumoral cells are outside GTV2. We initialize the mechanical component of our model with GTV1 and the diffusion component with GTV2. As the model includes white fiber direction (see below) known to influence tumor growth, it is essential to delineate GTV1 on MRI-T1i and GTV2 in MRI-T2 accurately.

Atlas

Practically, our atlas consists of two images. One is an MR image. The other is an image of labels where each color corresponds to an identified structure. We chose to use an artificial MRI, generated by the brainweb (Cocosco *et al* 1997) software. To minimize partial volume effects when matching, a high-definition MRI with smaller voxels than that of our patient's MRI was used.

An expert identified the contours for each cerebral structure of interest on this artificial MR image (Bondiau 2005). Since our primary interest was tumor growth, we focused on structures that were relevant to this application. Such structures with particular behavior were the skull, the ventricular system, the gray matter (including basal ganglia), the white matter and the falx, according to the anatomical data of the atlas of Jean Talairach (Talairach and Tournoux 1998). After delineation, these structures were transformed into tetrahedral meshes from which we simulated tumor growth, i.e., the tumor cells diffusion coupled with mechanical interactions between tumor with the surrounding anatomical structures.

It is noteworthy that GBM is a tumor of glial origin that expands preferentially towards the direction of white fibers (Price *et al* 2003). To better estimate direction and speed, data from diffusion tensor imaging (DTI) were used in the white matter. This DTI is generic and does not apply for this particular patient, it describes the anisotropic diffusion of water molecules in normal brain tissues and thus gives an estimate of white fiber directions. DTI images were coupled with the atlas. Ultimately, the complete simulation process was performed in the high-resolution MRI and DTI. The characteristics of the atlas image are shown in table 2.

Mathematical model

This model corresponds to our tumor partition into two volumes: GTV1 and GTV2. GTV1 is more closely associated with the proliferation component than with the diffusion component. It is responsible for the mechanical volume effect on the brain. By adding new cells, GTV1 pushes away surrounding structures. GTV2 is more closely associated with the diffusion component. It invades adjacent structures and is responsible for an infiltration of the white and gray matter. This component expands faster than that of GTV1 but has a smaller volume effect than the proliferation component.

Calibration with patient's image was used to estimate two quantities: geometrical displacements of each structure (i.e. deformations) and tumor cell density. The mathematical equations on which our model was set are described below.

Mechanical model. We used the classical linear elasticity theory to describe the behavior of the brain parenchyma (Fung 1993). Since the growing process is very slow, we assume that the relation was linear. Thus at every point of the brain, the stress is related to the strain by

$$\sigma = k\varepsilon \quad (3)$$

Table 3. Parameters of the brain model.

Structures	Elasticity (mechanical)	Diffusion
Ventricles	0	0
White matter	1000 Pa	MRI Diffusion Tensor
Gray matter	1000 Pa	1/10 of max of MRI diffusion tensor
Skull	Infinite	0
Falx cerebri	100 000	0

where σ is the stress tensor, k is the elasticity of the brain and ε is the linearized Lagrange strain tensor defined by

$$\varepsilon = \frac{1}{2}(\nabla\chi + \nabla\chi^t) \quad (4)$$

where χ and ∇ are the displacement of the point considered and the gradient operator.

Then the mechanical equilibrium relation can be written as follows:

$$\operatorname{div} \sigma + F_e = 0 \quad (5)$$

where F_e is the external forces on the brain.

Since the different brain structures do not react the same way to GBM growth, we incorporated different mechanical characteristics for these different structures. The atlas was enriched with particular parameters of elasticity for white and gray matter, skull and falx (see table 3 for values) in order to obtain a mechanical model of the brain. These parameters were estimated in (Miga *et al* 2000). As the atlas includes these parameters, they are the same from one patient to the other.

Diffusion model. We used the diffusion equation proposed by Murray in 1989 (Murray 1989):

$$\underbrace{\frac{\partial c}{\partial t}}_{\text{Tumor rate evolution}} = \underbrace{\operatorname{div}(D\nabla c)}_{\text{Diffusion factor}} + \underbrace{\rho c}_{\text{Source factor}} \quad (6)$$

where c represents the normalized cell density (c varies from 0 to 1). The real cell density C is obtained by multiplying c with the carrying capacity of the tissue C_{\max} (GTV1) estimated to be equal to 3.5×10^4 cells mm^{-3} (Cruywagen *et al* 1995). D represents the diffusion tensor defining the mobility of the glioma cells. The source factor, ρc , reflects tumor aggressiveness. As our model has particular parameters of elasticity for ventricles, white and gray matter, skull and falx, we assigned different diffusion values for these structures. The local behavior of the tumor depends only on the diffusion tensor D and the source factor ρ (see figure 4 for the different diffusion behavior). By changing the source factor, a high tumor aggressiveness can be simulated which corresponds to clinical experience. We consider including this aggressiveness value if it could be predicted by pathology specimens and/or biopsy.

The tumor also acts as an inner mechanical pressure correlated with tissue tumor density. Diffusion of tumor cells along white fibers modifies tumor spread which, in turn, affects mechanical modification. In this first approach, we did not take in account this phenomenon.

Noteworthy, this simulation process runs in a quarter of an hour in a PC equipped with a single CPU at 2 GHz.

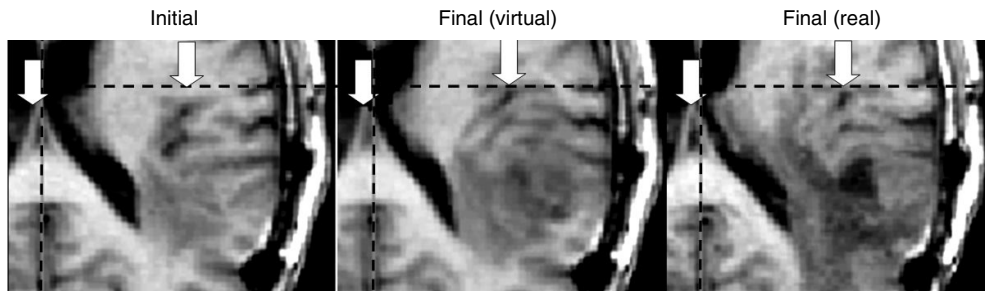


Figure 3. Mechanical effect of tumor growth, frontal view. Left: original patient MRI. Middle: simulated final MRI. Right: final patient MRI. This image only shows the tumor growth effect on other brain structures. See the deformations of the left ventricle. Diffusion was not taken into account for this image.

Practical issues

Model initialization. There are different evolutions of glioblastoma, some will have a higher diffusion component than a proliferate rate, and other will have a higher proliferate rate than diffusion. For that reason, our model needs to be initialized with GTV1 and GTV2 initial contours. The model then predicts the expected GTV1 and GTV2 contours, together with structure deformations and tumor cell density.

For educational purposes, any initialization shape can be performed. It is also interesting to simulate individualized growth. To that end, we co-aligned patient's images where GTV1 and GTV2 had been delineated with an atlas image, so that the two contours were easily registered onto the atlas.

Numerical issues. We used a linear tetrahedron element to discretize our computation domain is represented by a mesh of 250 000 tetrahedra. Using the finite element theory, equations (3)–(5) can be transformed into linear systems with deformation, X , and tumor cell density, c , as variables. We use MATLAB[®] software⁵ for this part of the work. These systems are then repeatedly solved by short time steps, until tumor growth yields the final expected time.

Results

To test our model, we compared its results with tumor growth as observed on patient final images. Model initialization was performed on a tumor recurrence visible on MRI. These volumes were compared to a second MRI, performed six months later, on which interval growth was estimated. To enable a comparison, estimated deformations as well as tumor cell density were reported on the initial MRI, yielding a virtual image that would correspond to six months of growth in our model. We first present the results of the mechanical model (diffusion expansion is set to 0), then the results of the diffusion model (mechanical expansion is set to 0), and finally the results of the complete model. See figure 7 for complete 3D results.

Results of the mechanical model

Our results for the mechanical model are shown in an axial plane in figure 3. The result of the simulation of brain deformation must be compared with the patient's MRI done six months

⁵ <http://www.mathworks.com/>.

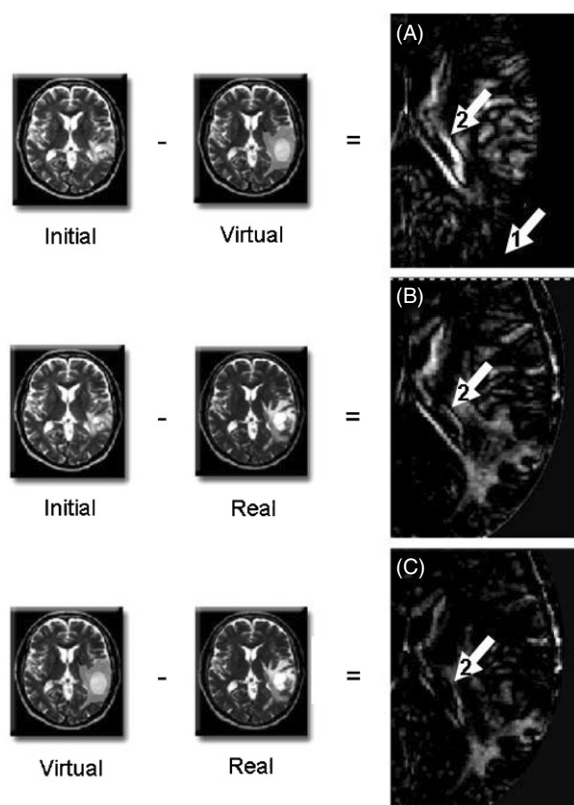


Figure 4. Up: images differences between initial image and virtual image, for the skull area (arrow 1), the result is black meaning there is no difference, but in the ventricle area (arrow 2 in image A) the result is white meaning there is high difference. Middle: images differences between initial image and real image of patient (six months later), in the ventricle area (arrow 2 in image B) the result is white meaning there is high difference. Down: images differences between final virtual and real patient image (six months later), in the ventricle area (arrow 2 in image C) the result is dark gray meaning there is light difference the ventricle in C. Image differences are normalized on initial image.

later. The deformations simulated by the model were applied to initial MRI data to simulate a virtual MR image (the diffusion results are not reported; thus tumor shapes are not comparable between the virtual and the patient's MRI). The displacements of the different brain structures observed on virtual images are in good agreement with the deformations observed on patient's MRI at six months. Deformations of the left ventricle and the deformation of sulci can be seen in the middle and left images of figure 3, and the tumor mass effect can be appreciated.

We compute image differences (ID) between initial images, virtual images and patient image six months later; the results are shown in figure 4. Difference images are normalized relative to the initial image. We compute for each 3 image; histogram, average, odds ratio of intensity of pixels. The results are shown in table 4. The average and the odd ration of ID between virtual and real image is lower than between initial and virtual or initial and real.

In order to quantify the accuracy of the simulation, an expert manually selected corresponding feature points on the first patient MRI (see figure 5), on the six months later simulated MRI and in the six months later real MRI. The measured displacements of these

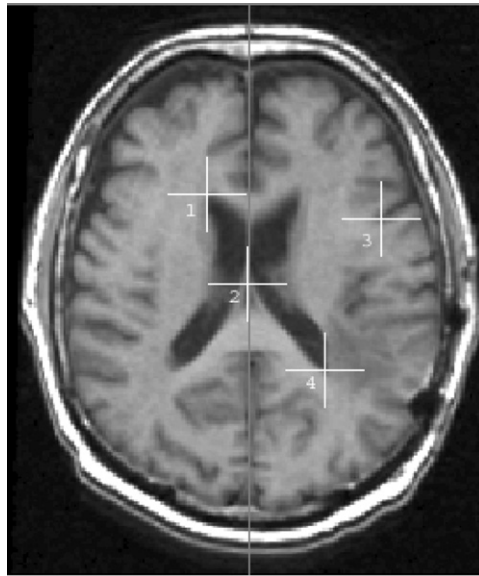


Figure 5. Position of the selected landmark in initial MRI.

Table 4. Comparison between the measured displacements and the simulated ones on four landmarks.

Image difference	Initial–virtual	Initial–real	Real–virtual
Average	26	27	21
Odds ratio	38, 52	34	26
Number of pixel analyzed	30 000	30 000	30 000

Table 5.

Point	(x, y) initial A	(x, y) final virtual B	(x, y) final real C	Distance A–B D	Distance A–C E	Distance B–C F
Unit	voxel	voxel	voxel	mm	mm	mm
1	(113, 109)	(113, 108)	(112, 108)	0.60	0.85	0.60
2	(136, 159)	(134, 159)	(134, 156)	1.20	2.17	1.80
3	(212, 122)	(210, 120)	(211, 120)	1.70	1.34	0.60
4	(180, 208)	(174, 211)	(176, 210)	4.03	2.68	1.34
			Mean	1.88	1.76	1.09

points in six months can be compared to those simulated by the model. See table 5 for the results.

Results of the diffusion model

The result of the diffusion model is shown in figure 6. There is no deformation of brain structures in this figure; only the progression of the tumor diffusion is represented. This result can be compared with patient MRI six months later. The introduction of the white fiber directions allows for a simulation of the VG that is in good agreement with that observed on patient's images.

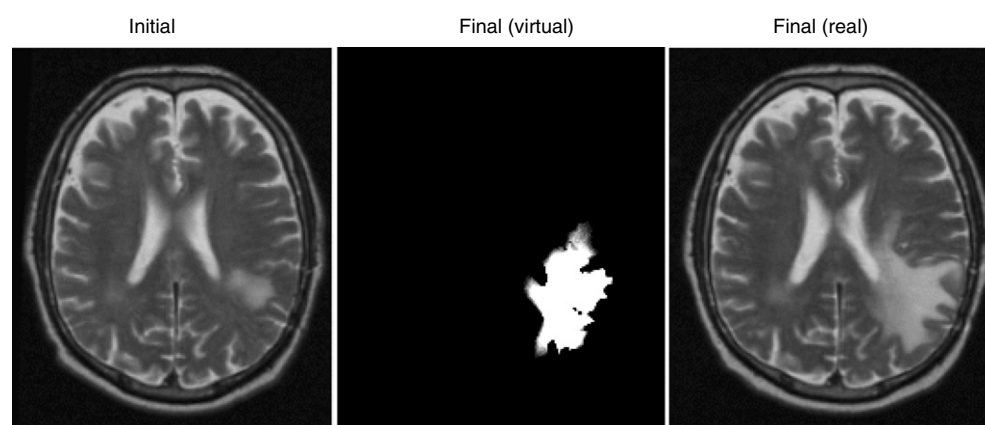


Figure 6. Diffusion effect of tumor growth, axial view. Left: original patient MRI. Middle: simulated final tumor. Right: final patient MRI.

Combined mechanical and diffusion models

In the first part of this work, images were computed in the model. We computed a new GTV2 each month, so that we could compare the changes of GTV2 during the simulation steps. The initial, final virtual and final real volumes of GTV1 are 810, 12384 and 15120 mm³, respectively. The GTV2 volume in the virtual final MRI is a ‘rate of tumor’ cell and we cannot compute a volume and make a comparison with real images as we do not know the ‘rate of tumor’ in real images. The size of GTV2 in the initial and real final images is 27.10³ and 112.10³ mm³, respectively.

The second part of this work shows the definitive results: the model (with GTV1 and GTV2) is matched with patient’s MRI, after adding mechanical and diffusion components, and interaction between the two components. Computing details are presented in the following footnote⁶. Figure 7 shows results with different isolevels of diffusion with the mechanical component superimposed with patient T2 MRI made six months later.

Discussion

The diffusion tensor imaging reflects the preferred direction of water movement and tumor cells moves in the direction of water. The use of DTI to predict the future position of tumor cells represents the main improvement of our model compared to other tumor growth models and the results are promising. Simulated images are in good agreement with the patient real image performed six months later, which can be considered as ground truth. It is critical to use a reliable parameter set during simulation. In this work, we tuned our parameter set to get a correct visual agreement, so that it is possible that different parameter sets apply to different tumors. However, our model still has some default. For example, modification of fiber structure composing the white matter in the vicinity of the tumor can have an effect on the diffusion component. To our knowledge, the process governing this modification is not well understood, and its modeling still remains a challenge.

The advantages of performing simulations of tumor growth are multiple. It may be helpful to classify tumors with respect to their aggressiveness which can be estimated with some hidden parameters (the ρ of the source factor ρc): given two images, these hidden parameters can be

⁶ <http://www.inria.fr/rrrt/rr-5187.html>.

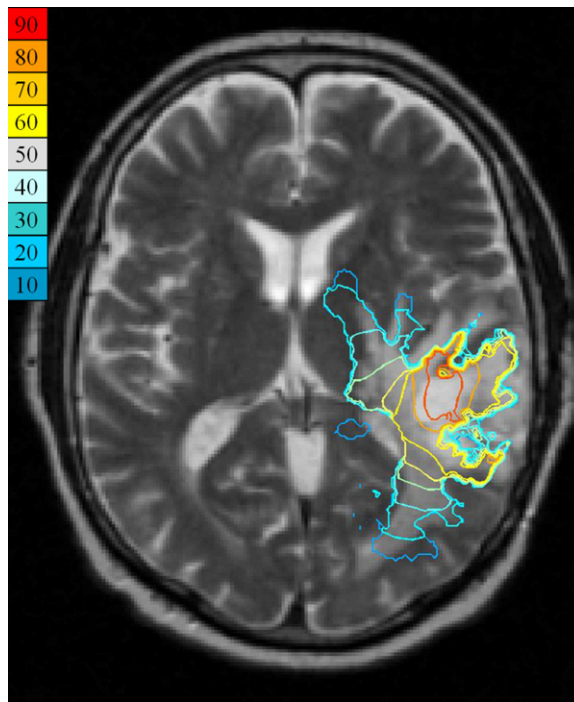


Figure 7. Results of the mechanical effect and diffusion of tumoral growth in T2 MRI made six month later. Superimposed color bands represent iso-level of the predicted tumor cells concentration in percent. See the correct simulation of tumor growth in white matter, in white fibers direction and the prediction of invasion at six months.

estimated as those obtained in the most realistic and reproducible simulation. Tumor growth simulation could also help to improve focal treatment delivery for surgery or radiotherapy and thus improve the definition of invasion margins (by tumor cell density estimation). It may also serve for educational or scientific purposes.

Patient tumor growth rate

The numerical model can be used to quantify 3D invasion of GBM in a patient's brain. This approach can be used to establish a growth rate for a GBM. Since tumors can exhibit different growth rates, the diffusion of some lesions can be more extensive than for others, due to a higher 'aggressiveness'. In these cases, a high diffusion component may dominate over the mechanical component, resulting in a faster GTV2 growth. A reasonable range of parameters can be determined. However, an accurate estimation of parameters prediction for aggressiveness or tumor behavior (rate of tumor cell density) may be extracted from a biopsy or pathology examination. Estimation of this aggressiveness would help to guide therapeutic decisions, since tumors with a weak rate of diffusion can benefit from resection surgery (Burgess *et al* 1997). Moreover, the simulation could help to predict the clinical outcome.

Radiotherapy margins

In radiotherapy treatments, the delineation of the clinical target volume (CTV) must take into account the probability that isolated malignant cells may be present in the edema surrounding

the tumor or in the adjacent brain structures. Some isolated malignant cells may have not yet generated an edema and thus cannot be seen in T2 MRI. Presently, more than 90% of local recurrences are within the irradiation fields (Wallner *et al* 1989, Gaspar *et al* 1992) or marginal (i.e. on borders) and dose escalation seems reasonable (Lee *et al* 1999b). By estimating tumor cell density, our approach could help to define a risk that malignant cells are present, and thus help to delineate the CTV and respect brain matter. This could conduce to propose a clinical study of delivering a localized high dose of radiation in the predicted recurrence area.

Furthermore, segmentation of GTV1 and GTV2 was based on pre-therapeutic MRI and it is possible that the tumor still grows after the MRI and before treatment. In this case, the VG would help to predict locoregional spread at the time of treatment.

After treatment for GBM, recurrences usually occur within 1 year (on average). The image of radionecrosis, a well-know radiotherapy complication, might be difficult to distinguish from a recurrence image, but the growth patterns are different. VG growth simulation may help to distinguish between radionecrosis and recurrence.

Educational issues

This model was originally developed in order to investigate the development of brain tumors and to study multidimensional features such as proliferation and invasion at the same time. This type of tumor growth simulator could be of great interest to learning the mechanisms underlying GBM spread. 3D visualization of tumor growth helps to understand the preference for white matter, and why some tumors propagate into gray matter. This could lead to a better comprehension of tumor growth.

Patients can present with symptoms related to a damaged brain area although the tumor was absent in this area on the initial MRI. This can be explained by microscopic invasion of these areas by tumor (i.e. not yet seen on the MRI). In this case, the predictive computation of tumor spread computation of future development of the tumor in this area would help to predict clinical outcome and symptoms.

Improving the model

Simulating GBM growth is complex, associating mechanical and diffusion components. The model could be personalized by bringing more individual information: for instance, the patient DT image or the tumor growth rate could be estimated by other means (biopsy and pathology examination).

Conclusion

Glial tumors can be represented by two components: a proliferative component with a mass effect on other brain structures and an invasive component infiltrating brain structures. In this work, we simulated GBM growth by coupling these two components. This growth was simulated on a virtual image (an atlas), where different structures of interest had been delineated. The 'introduction' of white fiber directions, by using a DT image, improves the realism of the diffusion component.

The results of our simulation have shown a good correlation with tumor growth as observed on an MRI patient. Different tumor aggressiveness can also be simulated by tuning additional parameters. This work has demonstrated that modeling the complex behavior of brain tumors is feasible and will account for further validation of this new conceptual approach.

The applications of this model are numerous: estimation of the microscopic invasion for a better definition of margins (for surgery or radiotherapy purposes), estimation of tumor aggressiveness for classification purposes, education, etc. The model does not require specific imaging protocols. Routine imaging, such as MRI, sequences were sufficient for such purposes.

This model was initialized on patient data, leading to realistic and promising but still preliminary results.

References

- Bondiau P Y *et al* 2005 Atlas-based automatic segmentation of MR images: validation study on the brainstem in radiotherapy context *Int. J. Radiat. Oncol. Biol. Phys.* **61** 289–98
- Burgess P K, Kulesa P M, Murray J D and Alvord E C Jr 1997 The interaction of growth rates and diffusion coefficients in a three-dimensional mathematical model of gliomas *J. Neuropathol. Exp. Neurol.* **56** 704–13
- Bussemaker H, Deutsch A and Geigant E 1997 Mean-field analysis of a dynamical phase transition in a cellular automaton model for collective motion *Phys. Rev. Lett.* **78** 5018–21
- Cococco C A, Kollokian V, Kwan R K-S and Evans A C 1997 BrainWeb Online interface to a 3D MRI simulated brain database *NeuroImage* **5** 425
- Cruywagen C, Woodward D E, Tracqui P, Bartoo G T, Murray J D and Alvord E C 1995 The modelling of diffusive tumours *J. Biol. Syst.* **3** 937–45
- Deisboeck T S, Berens M E, Kansal A R, Torquato S, Stemmer-Rachamimov A O and Chiocca E A 2001 Pattern of self-organization in tumor systems : complex growth dynamics in a novel brain tumour spheroid model *Cell Prolif.* **34** 115–34
- Fazeny-Dorner B, Wenzel C, Veitl M, Piribauer M, Rossler K, Dieckmann K, Ungersbock K and Marosi C 2003 Survival and prognostic factors of patients with unresectable glioblastoma multiforme *Anticancer Drugs* **14** 305–12
- Frenay M, Lebrun C, Lonjon M, Bondiau P Y and Chatel M 2000 Up-front chemotherapy with fotemustine (F)/cisplatin (CDDP)/etoposide (VP16) regimen in the treatment of 33 non-removable glioblastomas *Eur. J. Cancer* **36** 1026–31
- Fung Y C 1993 *Biomechanics, Mechanical Properties of Living Tissues* (Berlin: Springer)
- Gaspar L E, Fisher B J, Macdonald D R, LeBer D V, Halperin E C, Schold S C Jr and Cairncross J G 1992 Supratentorial malignant glioma: patterns of recurrence and implications for external beam local treatment *Int. J. Radiat. Oncol. Biol. Phys.* **24** 55–7
- Jeremic B, Milicic B, Grujicic D, Dagovic A and Aleksandrovic J 2003 Multivariate analysis of clinical prognostic factors in patients with glioblastoma multiforme treated with a combined modality approach *J. Cancer Res. Clin. Oncol.* **129** 477–84
- Kansal A R, Torquato S, Chiocca E A and Deisboeck T S 2000a Emergence of a subpopulation in a computational model of tumour growth *J. Theor. Biol.* **207** 431–41
- Kansal A R, Torquato S, Harsh G R IV, Chiocca E A and Deisboeck T S 2000b Simulated brain tumour growth dynamics using a three-dimensional cellular automaton *J. Theor. Biol.* **203** 367–82
- Kansal A R, Torquato S, Chiocca E A and Deisboeck T S 2000c 1 Emergence of a subpopulation in a computational model of tumour growth *J. Theor. Biol.* **207** 431–41
- Kansal A R, Torquato S, Harsh GR IV, Chiocca E A and Deisboeck T S 2000d Cellular automaton of idealized brain tumour growth dynamics *Biosyst.* **55** 119–27
- Kantor G, Loiseau H, Vital A and Mazon J J 2001 Gross tumor volume and clinical target volume in adult gliomas *Cancer Radiother.* **5** 571–80
- Kyriacou S K, Davatzikos C, Zinreich S J and Bryan R N 1999 Nonlinear elastic registration of brain images with tumour pathology using a biomechanical model *IEEE Trans. Med. Imaging* **18** 580–92
- Lee S W *et al* 1999a Patterns of failure following high-dose 3-D conformal radiotherapy for high-grade astrocytomas : a quantitative dosimetric study *Int. J. Radiat. Oncol. Biol. Phys.* **43** 79–88
- Lee S W, Fraass B A, Marsh L H, Herbort K, Gebarski S S, Martel M K, Radany E H, Lichter A S and Sandler H M 1999b Patterns of failure following high-dose 3D conformal radiotherapy for high-grade astrocytomas: a quantitative dosimetric study *Int. J. Radiat. Oncol. Biol. Phys.* **43** 79–88
- Legler J M, Ries L A, Smith M A, Warren J L, Heineman E F, Kaplan R S and Linet M S 1999 Brain and other central nervous system cancers : recent trends in incidence and mortality *J. Natl. Cancer Inst.* **91** 1382–1390

- Miga M, Paulsen K, Kennedy F, Hoopes P, Hartov A and Roberts D 2000 *In vivo* analysis of heterogeneous brain deformation computation for model updated image guidance *Comput. Methods Biomech. Biomed. Eng.* **3** 129–46
- Mineo J F, Bordron A, Baroncini M, Ramirez C, Maurage C A, Blond S and Dam-Hieu P 2007 Prognosis factors of survival in GBM multiforme: a multivariate analysis of 340 patients *Acta. Neurochir.* **2**
- Miralbell R *et al* 1999 European organization for research and treatment of cancer trial 22933 *J. Clin. Oncol.* **17** 3143–9
- Murray J D 1989 *Mathematical Biology* (Heidelberg: Springer)
- Murray J 2002 *Mathematical Biology* (Berlin: Springer)
- Nakagawa K *et al* 1998 High-dose conformal radiotherapy influenced the pattern of failure but did not improve survival in GBM multiforme *Int. J. Radiat. Oncol. Biol. Phys.* **40** 1141–9
- Patel A A, Gawlinski E T, Lemieux S K and Gatenby R A 2001 A cellular automaton model of early tumour growth and invasion *J. Theor. Biol.* **7** 315–31
- Price S J, Burnet N G, Donovan T, Green H A, Pena A, Antoun N M, Pickard J D, Carpenter T A and Gillard J H 2003 Diffusion tensor imaging of brain tumours at 3T: a potential tool for assessing white matter tract invasion? *Clin. Radiol.* **58** 455–62
- Retsky M W, Swartzendruber D E, Wardwell R H and Bame P D 1990 Is Gompertzian or exponential kinetics a valid description of individual human cancer growth? *Med. Hypotheses* **33** 95–106
- Ruiz-Alzola J, Westin C F, Warfield S K, Alberola C, Maier S and Kikinis R 2002 Nonrigid registration of 3D tensor medical data *Med. Image Anal.* **6** 143–61
- Swanson K R, Alvord E C Jr and Murray J D 2002a Virtual brain tumors (gliomas) enhance the reality of medical imaging and highlight inadequacies of current therapy *Br. J. Cancer* **86** 14–8
- Swanson K R, Alvord E C Jr and Murray J D 2002b Quantifying efficacy of chemotherapy of brain tumours with homogeneous and heterogeneous drug delivery *Acta Biotheor.* **50** 223–37
- Swanson K R, Alvord E and Murray J 2002c Virtual brain tumor (glioma) enhance the reality of medical imaging and highlight inadequacies of current therapy *Br. J. Cancer* **86** 14–8
- Talairach J and Tournoux P 1998 *Co-planar Stereotaxic Atlas of the Human Brain, 3D Proportion System, an Approach to Cerebral Imaging* (Stuttgart: Georg Thieme) Nov 1988-130 illustrations
- Tracqui P 1995 From passive diffusion to active cellular migration in mathematical models of tumour invasion *Acta Biotheor.* **43** 443–64
- Tracqui P, Cruywagen G C, Woodward D E, Bartoo G T, Murray J D and Alvord E C Jr 1995 A mathematical model of glioma growth: the effect of chemotherapy on spatio-temporal growth *Cell Prolif.* **28** 17–31
- Wallner K E, Galicich J H, Krol G, Arbit E and Malkin M G 1989 Patterns of failure following treatment for glioblastoma multiforme and anaplastic astrocytoma *Int. J. Radiat. Oncol. Biol. Phys.* **16** 1405–9
- Wolff J E, Trilling T, Molenkamp G, Egeler R M and Jurgens H 1999 Chemosensitivity of glioma cells *in vitro*: a meta analysis *J. Cancer Res. Clin. Oncol.* **125** 481–6
- Woodward D E, Cook J, Tracqui P, Cruywagen G C, Murray J D and Alvord E C 1996 A mathematical model of glioma growth: the effect of extent of surgical resection *J. Cell Prolif.* **29** 269–88